Elastic properties of single-crystal NiF_2 †

Adam Yu Wu*
Department of Physics, The University of Chicago, Chicago, Illinois 60637
(Received 14 August 1975; revised manuscript received 19 January 1976)

The elastic properties of NiF_2 were studied at $65 < T < 300$ K using the ultrasonic pulse superposition method. At 300 K, the measured adiabatic elastic stiffness moduli, in units of 10^{11} dyn/cm^2, are $C_{11}=14.50$, $C_{12}=11.04$, $C_{13}=9.09$, $C_{33}=22.08$, $C_{44}=4.65$, and $C_{66}=9.94$. The measured moduli are compared with the theoretical values calculated from Pandey's model by using published Raman frequencies. Near 300 K, each dC_{ij}/dT has a negative value. But dC_S/dT, where $C_S=\frac{1}{2}(C_{11}-C_{12})$, is positive between 300 K and the Nêel temperature T_N. Other anomalous features are the following. There is a long precursor above T_N in C_{33} and C_{44}, C_{33} exhibits critical exponents near T_N, whereas the values of C_{11}, C_{66}, C_S, etc. show sharp "cut-off" anomalies below T_N. These can be eliminated by a 4-kOe magnetic field along suitable directions. These properties of the elastic moduli are discussed in terms of a lattice instability or volume magnetostrictive coupling mechanism above T_N, linear magnetoelastic couplings, shear instability, and weak ferromagnetic domain effects, respectively. Possible existence of twin domains is proposed.

I. INTRODUCTION

In recent years, ultrasonic methods such as phase comparison[1] and pulse superposition[2] have become powerful tools for studying physical properties in materials. The high resolution of these methods enables one to detect small changes in acoustic velocities. Physical properties such as anomalies in acoustic velocities, attenuation, critical phenomena, and various coupling mechanisms in the crystal can be studied. Experiments of this sort have been reported in literature,[3,4] but the present study is one of the few to report the complete elastic tensor of a weak ferromagnet over a large temperature range.

NiF_2 has been chosen for this study for several reasons. First, it has the important crystal structure of rutile (TiO_2). The lattice dynamics of this type of crystal has become a subject of interest recently.[5] Second, NiF_2 becomes a canted weak ferromagnet below its Nêel temperature T_N.[6,7] The properties of this type of phase transition are very important for building up the theory of magnetism. Very few ultrasonic experiments have been done on such substances.[8] Third, NiF_2 also exhibits a crystallographic distortion below T_N.[9] In view of the above, we feel that a systematic measurement of acoustic velocities in NiF_2 is needed to understand more about the lattice dynamics, phase transition, weak ferromagnetism, and domain effects in this crystal.

We measured a complete set of the adiabatic stiffness moduli of NiF_2 in the temperature range $65<T<300$ K. From these moduli and their behavior in a magnetic field, the associated elastic properties are investigated. In the following, we briefly review the crystal properties. The details of the experimental procedures and the results are presented in Secs. III and IV, respectively. The discussions and the conclusions of the experiments are presented in Sec. V.

II. CRYSTAL PROPERTIES

NiF_2 has the rutile-type crystal structure at room temperature. It belongs to the space group $P4_2/mnm$. The tetragonal unit cell is shown in Fig. 1. It contains six ions: Two nickel ions are located at positions $(0,0,0)$ and $(\frac{1}{2},\frac{1}{2},\frac{1}{2})$, and four fluorine ions at positions $(u,u,0)$, $(1-u,1-u,0)$ and $(\frac{1}{2}\pm u,\frac{1}{2}\mp u,0)$. The lattice constants are $a=b=4.6506\pm0.0002$ Å and $c=3.0836\pm0.0004$ Å, and the lattice parameter is $u=0.302$.[10] The density determined from these values are 4.815 g/cm^3.

Below $T_N=73.2$ K, NiF_2 is a weak ferromagnet. Its magnetic properties can be explained by a two-sublattice model[7] in which the corner and body-centered spins of the nickel ions lie nearly antiparallel in the a-b plane but are canted slightly away from the b axis, resulting in a weak moment pointing along the a direction. The weak ferromagnetic moment can point along four equivalent directions in the a-b plane, giving rise to four possible directions of the domains. It has been shown[9] that in zero magnetic field, the averaged values of the a and b lattice constants are equal, but in the presence of a magnetic field which causes the domains to line up along the a direction (so defined), the lattice constant a is greater than the lattice constant b by 0.026% at 20.4 K.[9] A single domain NiF_2 crystal belongs to the orthorhombic magnetic space group $Pnn'm'$.[11]

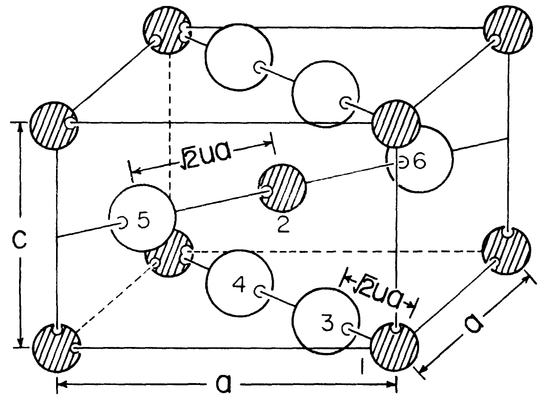

FIG. 1. Rutile-type crystal structure of NiF_2 at room temperature. It has a tetragonal unit cell containing six ions. The black balls represent Ni^{++} ions and the white balls represent F^- ions. Ion 2′ just below ion 2 along the c axis is not shown.

III. EXPERIMENTAL DETAILS

A. Specimen preparation

One large specimen cut from a single-crystal boule[12] was used for all the investigations. This specimen has a purity of 99.9% with Fe, Co, and excess Ni as main impurities. Two pairs of surfaces parallel to the (100) and (001) planes were prepared first. After the acoustic velocities for v_i, $i = 1-6$ were measured in the range $65 < T < 300$ K at 1 bar and at high pressures[13] at 296 K, another pair of surfaces parallel to the (110) plane was prepared for the measurements of v_7 to v_{10}. Finally, surfaces parallel to the (011) plane were prepared for measuring v_{11} and v_{12}. The designation of these velocity modes, their relations with the elastic stiffness moduli C_{ij}, and the thickness of the specimen are summarized in Table I.

TABLE I. Elastic modes, elastic stiffness moduli, and specimen lengths. [a]

Mode	Specimen length (cm) at 296 K	Velocity	ρv_i^2
$\vec{q}_L \parallel [100]$	$0.79374\underline{4}$	v_1	C_{11}
$\vec{q}_L \parallel [010]$	$0.79374\underline{4}$	v_2	C_{22}
$\vec{q}_L \parallel [001]$	$0.88428\underline{8}$	v_3	C_{33}
$\vec{q}_S \parallel [001]$, $\hat{e} \parallel [010]$	$0.88428\underline{8}$	v_4	C_{44}
$\vec{q}_S \parallel [001]$, $\hat{e} \parallel [100]$	$0.88428\underline{8}$	v_5	C_{55}
$\vec{q}_S \parallel [100]$, $\hat{e} \parallel [010]$	$0.79374\underline{4}$	v_6	C_{66}
$\vec{q}_L \perp (110)$	$0.67623\underline{3}$	v_7	$C_L = \frac{1}{2}(C_{11} + C_{12} + 2C_{66})$
$\vec{q}_S \perp (110)$, $\hat{e} \perp [001]$	$0.67623\underline{3}$	v_8	$C_S = \frac{1}{2}(C_{11} - C_{12})$
$\vec{q}_L \perp (101)$	$0.73782\underline{2}$	v_9	$C_{QL} = \frac{1}{2}(C_{11}l^2 + C_{33}n^2 + C_{55} + \{[C_{11}l^2 - C_{33}n^2 + C_{55}(n^2 - l^2)]^2 + 4l^2n^2(C_{13} + C_{55})^2\}^{1/2})$
$\vec{q}_L \perp (011)$	$0.73782\underline{2}$	v_{10}	$C'_{QL} = \frac{1}{2}(C_{22}m^2 + C_{33}n^2 + C_{44} + \{[C_{22}m^2 - C_{33}n^2 + C_{44}(n^2 - m^2)]^2 + 4m^2n^2(C_{23} + C_{44})^2\}^{1/2})$
$\vec{q}_S \perp (101)$, $\hat{e} \perp [010]$	$0.73782\underline{2}$	v_{11}	$C_{QS} = \frac{1}{2}(C_{11}l^2 + C_{33}n^2 + C_{55} - \{[C_{11}l^2 - C_{33}n^2 + C_{55}(n^2 - l^2)]^2 + 4l^2n^2(C_{13} + C_{55})^2\}^{1/2})$
$\vec{q}_S \perp (011)$, $\hat{e} \perp [100]$	$0.73782\underline{2}$	v_{12}	$C'_{QS} = \frac{1}{2}(C_{22}m^2 + C_{33}n^2 + C_{44} - \{[C_{22}m^2 - C_{33}n^2 + C_{44}(n^2 - m^2)]^2 + 4m^2n^2(C_{23} + C_{44})^2\}^{1/2})$

[a] $\vec{q}_L$ is the wave vector of the longitudinal propagations. $\vec{q}_S$ is the wave vector of the shear propagations. $\hat{e}$ is the particle vibration vector of the shear waves. (l, m, n) are the direction cosines of $\vec{q}$ with respect to the [100], [010], and [001] axes in the crystal.

The specimen was oriented by Laue back reflection to within 0.5° of the desired orientation. The required pair of polished surfaces were parallel to better than $\pm 5\times10^{-5}$ cm.

B. Ultrasonic experiments

The acoustic velocities were determined using the ultrasonic pulse superposition method.[2,14] The pulse repetition frequency was adjusted and recorded. The required $n=0$ condition was checked by using standard time markers exhibited with the video echo patterns displayed on a dual-trace oscilloscope, and by the method of tuning and detuning of the carrier frequencies as described by McSkimin.[2] A transit time change of a few parts in 10^{-6} can be detected.

The attenuation of acoustic waves for some modes have been measured near T_N using the pulse and echoes method. The amplitudes of the first two echoes displayed on the oscilloscope were measured. The absolute and relative accuracies of the attenuation were about 2 and 0.5 dB/cm, respectively.

C. Transducers and bonding

Coaxially gold plated X and AC cut quartz transducers of fundamental frequency 30 MHz, $\frac{1}{4}$ in. in diameter were used to generate longitudinal and shear modes, respectively. Dow Corning vacuum grease (No. 907V), Apiezon N grease and Dow Corning 705 fluid were used for the bond between the specimen and the transducer. For several modes, two kinds of bonds were necessary for studying the entire temperature range.

D. Low-temperature cryostat and specimen holder

The specimen was clamped to the end of a tapered copper plug. The plug fits in a chamber of a copper block which carries a heater wire. The rf signal wire and one of the copper-Constantan thermocouples are fed through holes in the plug to the transducer and specimen seat. Another thermocouple is imbedded in the block. The specimen assembly was lowered to the bottom of a stainless steel tube which has a long vacuum jacket. The tube was immersed in liquid nitrogen in a glass Dewar. The temperature was lowered to 65 K by pumping on the liquid nitrogen. Below 77.6 K, each data point was taken at a constant T achieved by controlling the pumping pressure on the liquid nitrogen and adjusting the power delivered to the heater. The relative accuracy of the temperature measurements was better than 0.02 K. Above 77.6 K, the measurements were done by slowly warming up the crystal at a rate less than 0.3 K/min.

E. Calculation of elastic moduli

Above T_N, NiF_2 is tetragonal and has six elastic stiffness moduli, $C_{11}, C_{12}, C_{13}, C_{33}, C_{44}$, and C_{66}. Below T_N, the magnetostriction lowers the crystal symmetry to orthorhombic and three more moduli, C_{22}, C_{55}, and C_{23} emerge. The relations among the acoustic velosities and C_{ij}'s are tabulated in Table I.[15]

When solving the quadratic equations for C_{13} or C_{23}, there are two possible roots for each. The correct choice was determined from Born's criterion of lattice stability[16] which requires that C_{ii} $(i=1-6)$, $C_{22}C_{33} - C_{23}^2$, and the determinent $\| C_{ij} \|$ $(i,j=1,2,3)$ be positive. In calculating the moduli, the x-ray lattice constant data of Haefner *et al.*[9] have been used to correct for changes in thickness and density with temperature.

F. Accuracy of measurements

The uncertainty in the measured velocities arises from several factors: (i) the non-reproducibility of the electronic measuring system; (ii) the changes in the quality, the coupling, and the thickness of the bonding; (iii) misorientations and impurities in the specimen; (iv) errors in the thickness, orientation, and the temperature determinations; (v) nonparallelism of surfaces; and (vi) other anharmonic and dissipative effects in the specimen. The uncertainty is estimated to be less than 0.2%.

IV. EXPERIMENTAL RESULTS

The directly measured elastic stiffness moduli at seven temperatures are summarized in Table II. Their T dependence in the range $65 < T < 300$ K in a zero magnetic field is plotted in Figs. 2–5. Their detailed behavior in a magnetic field $\vec{H}$ around T_N is plotted in Figs. 6–9. The absolute accuracy for these moduli is better than 0.3%. The relative accuracy is much better.

The modulus C_{12} obtained from C_L and C_S, and the moduli C_{13} and C_{23} obtained from C_{QL} and C_{QS} are also given in Table II. They are plotted in Fig. 10. The absolute accuracy of these is better than 0.8%.

The temperature derivatives listed in Table II were determined from the slopes of the smoothed curves at 300 K.

There is no amibiguity in the data above T_N. However, some explanation is needed for the data below T_N. As shown in the figures, there is very sharp "cutoff" anomaly in each of the modes C_{11}, C_{66}, C_L, C_S, and C_{QS} below T_N. At T_N, the acoustic velocity decreases very rapidly and the attenuation approaches infinity so that there is practically no

TABLE II. Directly measured and derived adiabatic elastic stiffness moduli of NiF_2 as a function of temperature (relative values).[a]

Elastic stiffness moduli	300	250	200	150	100	74	67	$\left(\frac{dX}{dT}\right)_{300\,K}$
C_{11}, C_{22}	14.50(±0.02)	14.59	14.68	14.75	14.82	14.85	14.87	−0.18
C_{33}	22.08(±0.02)	22.23	22.38	22.49	22.52	22.35	22.39	−0.33
C_{44}, C_{55}	4.652(±0.01)	4.665	4.675	4.681	4.679	4.675	4.671, 4.675	−0.03
C_{66}	9.94(±0.01)	10.06	10.17	10.27	10.36	10.40	···	−0.24
C_L	22.69(±0.02)	22.92	23.16	23.37	23.54	23.62	···	−0.47
C_S	1.722(±0.002)	1.701	1.676	1.652	1.629	1.624	1.623	0.05
C_{QL}, C'_{QL}	19.99(±0.02)	20.12	20.24	20.33	20.38	20.30	20.31, 20.30	−0.26
C_{QS}, C'_{QS}	4.410(±0.004)	4.427	4.442	4.452	4.452	4.437	4.445	−0.28
C_{12}	11.04(±0.04)	11.17	11.32	11.45	11.55	11.61	···	−0.28
C_{13}, C_{23}	9.08(±0.03)	9.15	9.23	9.36	9.36	9.36	···	−0.16

[a] Moduli are in units of 10^{11} dyn/cm^2, their absolute accuracies are given at 300 K. The temperature derivatives of these moduli at 300 K are in units of 10^9 dyn/cm^2 K. Data at 67 K were measured in a magnetic field along the a direction.

signal observable a few degrees below T_N down to 65 K. To show this phenomenon, the attenuation for several modes is plotted in Fig. 11. The cutoff anomaly in acoustic velocity and the attenuation for each mode could be removed by applying a magnetic field along certain definite directions. For instance, a magnetic field of 4 kOe along the a direction eliminates the anomaly in C_{11}, C_S, and C_{QS}, but not in C_{66} and C_L. For C_{66} and C_L, the anomaly can be removed by the same field along the [110] direction. These moduli restored by the magnetic field connect smoothly with their values above T_N. They can be regarded as the "intrinsic" moduli. In a weaker field, however, the anomali usually persisted. We may call these the "effective" moduli because in this case only the effective result from the strong magnetoelastic coupling in the specimen is observed, which will be discussed in Sec. V.

The "intrinsic" moduli in any one run showed no hysteresis as the temperature was lowered from 77.6 to 65 K and then increased from 65 to 77.6 K. But occasionally, the quality of the signal became poor or even vanished below T_N. The data presented in the figures are data for which the quality of the signal never deteriorated. The relative accu-

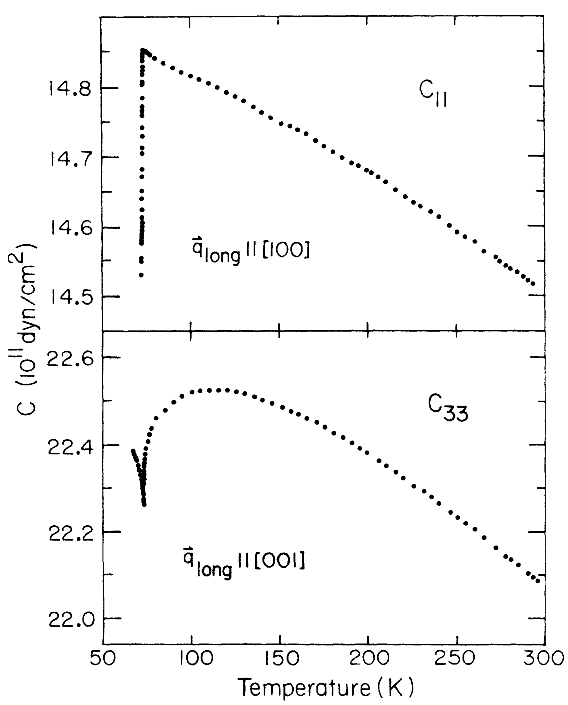

FIG. 2. Elastic stiffness moduli C_{11} and C_{33} vs temperature.

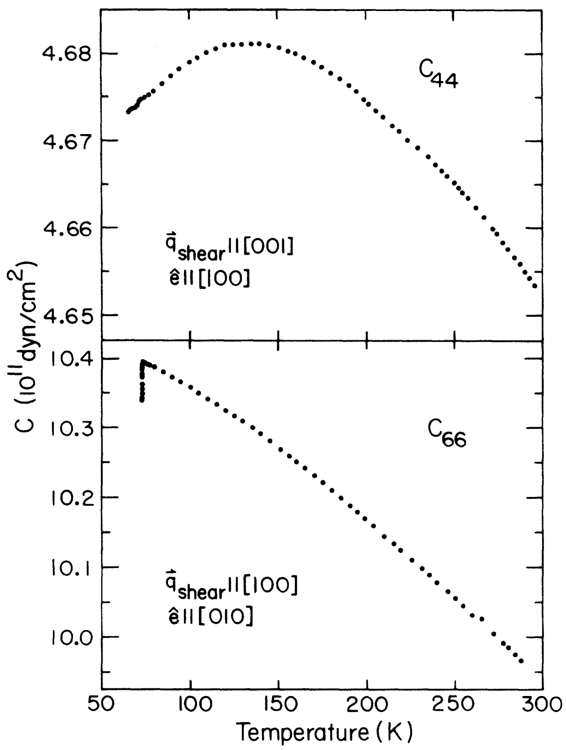

FIG. 3. Elastic stiffness moduli C_{44} and C_{66} vs temperature.

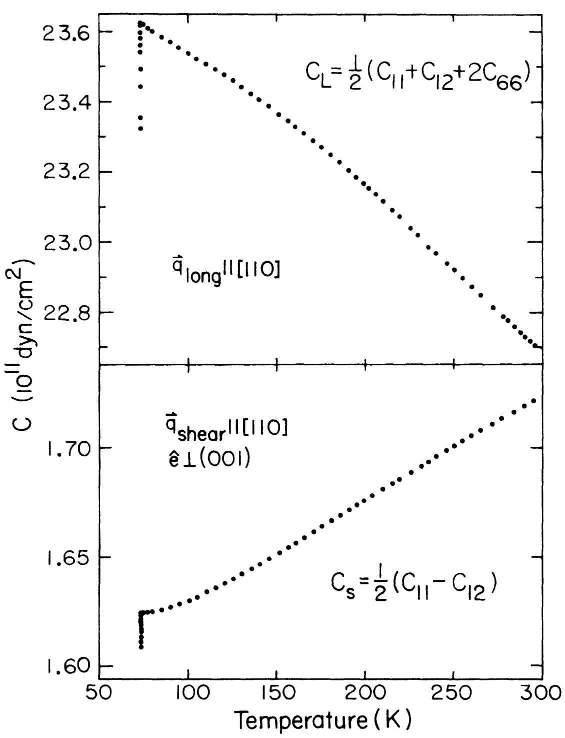

FIG. 4. Elastic stiffness moduli C_L and C_S vs temperature.

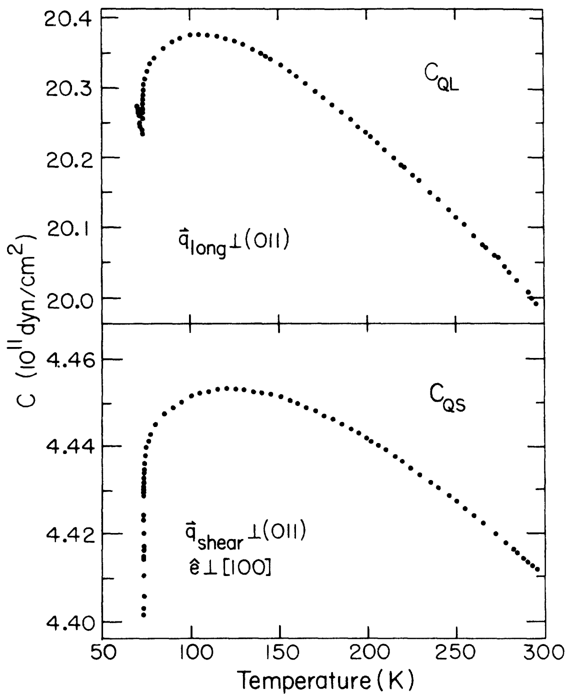

FIG. 5. Elastic stiffness moduli C_{QL} and C_{QS} vs temperature.

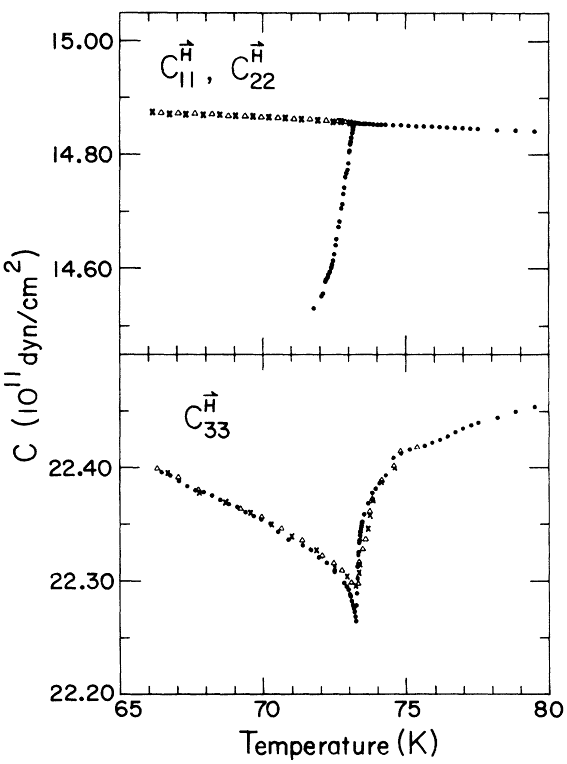

FIG. 6. Behavior of the elastic stiffness moduli C_{11}, C_{22}, and C_{33} in a magnetic field around T_N. ● represents data points in zero field. Upper diagram: (△) $\vec{q} \parallel [100]$, $\vec{H} \parallel [100]$; (×) $\vec{q} \parallel [010]$, $\vec{H} \parallel [100]$. Lower diagram: (△, ×) $\vec{q} \parallel [001]$, $\vec{H} \parallel [100]$, where $|\vec{H}| = 4$ kOe.

racy of the intrinsic moduli below T_N is a few parts in 10^6. For the effective moduli measured in small or zero field, the relative accuracy was less because of the rapid change of the velocities with temperature.

Three independent sets of measurements were taken for C_{44} above T_N for wave propagation along the [001], [100], and [110] directions with particle vibration along the [100], [001], and [001] directions, respectively. They all agree within the quoted accuracies. Below T_N, the first two results also agree with each other. Only one set of data is presented in Figs. 3 and 7. As shown, there is a 0.09% difference in C_{55} and C_{44} at 65 K due to the magnetoelastic coupling effect. Internal consistency of the moduli was also checked for all the other modes. They all agree within the quoted accuracies.

The elastic Debye temperature Θ_D (elastic) was determined to be 433 ± 6 K at room temperature, using the formula given by Betts *et al.*[17]

V. DISCUSSION

A. Theoretical elastic moduli

The elastic stiffness moduli can be determined from the force constants of the crystal.

Matossi has assigned seven force constants to rutile.[18] Referring to Fig. 1, four bond stretching force constants are k_1 (between the ion 2 and 5 or similar equivalent pairs), k_2 (between ions 2 and 3, etc.), k' (between ions 3 and 4, etc.), and k'' (between ions 3 and 5, etc.), and three bond bending force constants are d_1 (for ions 5, 2, and 6 to bend in the horizontal c plane), d_2 (for ions 5, 2, and 6 to bend in the vertical plane, etc.), and d_3 (acting among ions 2, 4, and 2′, etc.). These seven force constants can be explicitly expressed in terms of eighteen zone-center normal vibration frequencies. Using the Raman frequencies to determine these force constants, assuming $d_2 = d_3$, $k' = k''$, and introducing one more force constant k for the nearest-neighbor cation-cation interaction along the

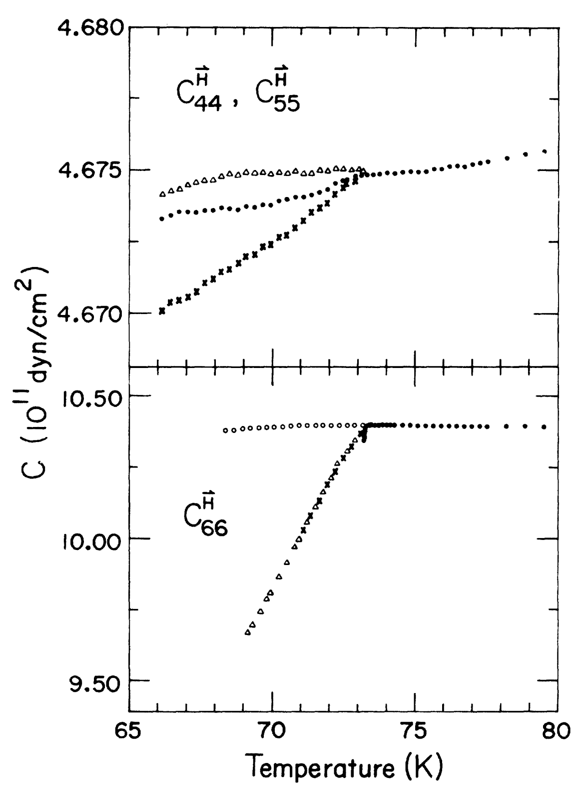

FIG. 7. Behavior of the elastic stiffness moduli C_{44}, C_{55}, and C_{66} in a magnetic field around T_N. ● represents data points in zero field. Upper diagram: (△) $\vec{q}\parallel[001]$, $\hat{e}\parallel[100]$, $\vec{H}\parallel[100]$; (×) $\vec{q}\parallel[001]$, $\hat{e}\parallel[010]$, $\vec{H}\parallel[100]$. Lower diagram: (△) $\vec{q}\parallel[100]$, $\hat{e}\parallel[010]$, $\vec{H}\parallel[100]$; (×) $\vec{q}\parallel[010]$, $\hat{e}\parallel[100]$, $\vec{H}\parallel[100]$; (○) $\vec{q}\perp(100)$, $\hat{e}\perp[001]$, $\vec{H}\parallel[110]$, where $|\vec{H}|=4$ kOe.

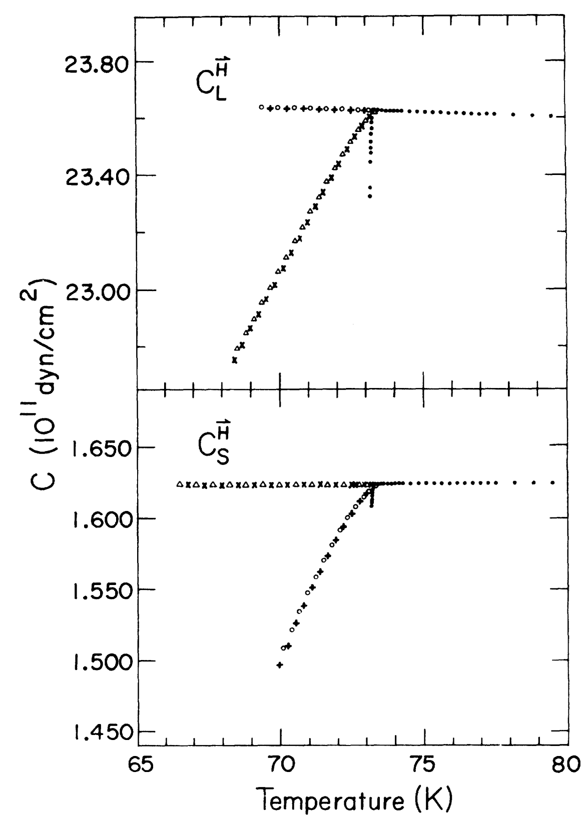

FIG. 8. Behavior of the elastic stiffness moduli C_L and C_s in a magnetic field around T_N. ● represents data points in zero field. Upper diagram: (△, ×) $\vec{q}\perp(110)$, $\hat{e}\perp(001)$, $\vec{H}\parallel[100]$; (○, +) $\vec{q}\parallel[110]$, $\hat{e}\perp(001)$, $\vec{H}\parallel[110]$. Lower diagram: (△, ×) $\vec{q}\perp(110)$, $\hat{e}\perp(001)$, $\vec{H}\parallel[100]$; (○, +) $\vec{q}\parallel[110]$, $\hat{e}\perp(001)$, $\vec{H}\parallel[110]$, where $|\vec{H}|=4$ kOe.

c direction, Pandey[19] was able to calculate the elastic stiffness moduli of rutile. The moduli of rutile[19] and MnF_2[20] calculated by his method, were found to agree well with experiments.

Applying Pandey's method to NiF_2 and adopting the reported Raman frequencies,[21] which are $\omega_1(A_{1g}) = 410$ cm^{-1}, $\omega_3(B_{1g}) = 70$ cm^{-1}, $\omega_4(B_{2g}) = 536$ cm^{-1}, and $\omega_5(E_g) = 305$ cm^{-1}, the force constants were determined as, in units of 10^5 dyn/cm, $k_1 = 1.095$ (the average value of the two k's determined from ω_1 and ω_4), $k_2 = 0.557$ (determined from ω_5), $k' = k'' = 0.166$ (determined from ω_3), and $k = 0.351$ (assigned). From these force constants, the moduli of NiF_2 were calculated. As we can see from the Table III (a), the calculated values for C_{11}, C_{33}, C_{12}, and C_{66} are in fair agreement with the experiments, but they are 43% too high for C_{44} and 29% too low for C_{13}. The discrepancies arise from the following. In Pandey's method, only the external strains are used for calculating the moduli, the internal strains are neglected. It has been shown by Striefler and Barsch[22] however that internal strains can contribute as much as 25% to the value of C_{44} in certain rutile-type crystals. If

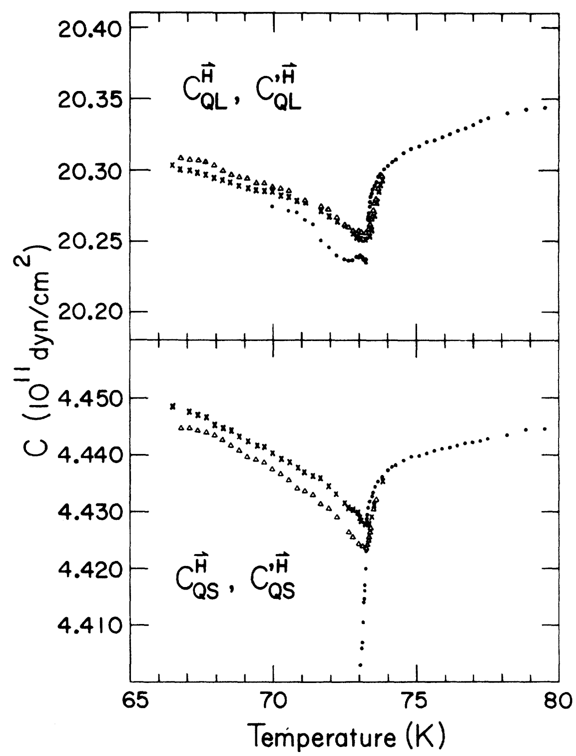

FIG. 9. Behavior of the elastic stiffness moduli C_{QL}, C'_{QL}, C_{QS}, and C'_{QS} in a magnetic field around T_N. ● represents data points in zero field. Upper diagram: (△) $\vec{q} \perp (101)$, $\vec{H} \parallel [100]$; (×) $\vec{q} \perp (011)$, $\vec{H} \parallel [100]$. Lower diagram: (△) $\vec{q} \perp (101)$, $\hat{e} \parallel [010]$, $\vec{H} \parallel [100]$; (×) $\vec{q} \perp (011)$, $\hat{e} \parallel [100]$, $\vec{H} \parallel [100]$, where $|\vec{H}| = 4$ kOe.

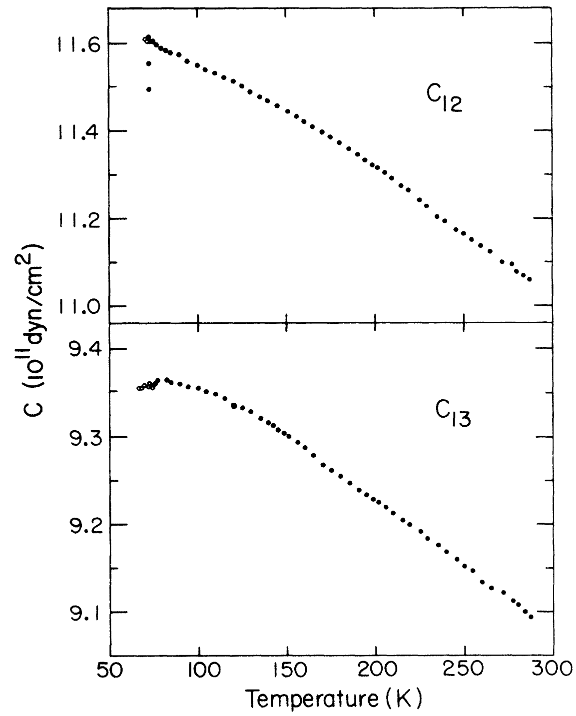

FIG. 10. Elastic stiffness moduli C_{12}, C_{13}, and C_{23} vs temperature. ● represents data points in zero field. ○ represents data points in a magnetic field of 4 kOe.

all seven force constants originally proposed by Matossi can be determined and used in the calculation, then the results might turn out more satisfactory. We note here that the Cauchy relations, $C_{12} = C_{66}$, $C_{13} = C_{44}$, are the result of central forces

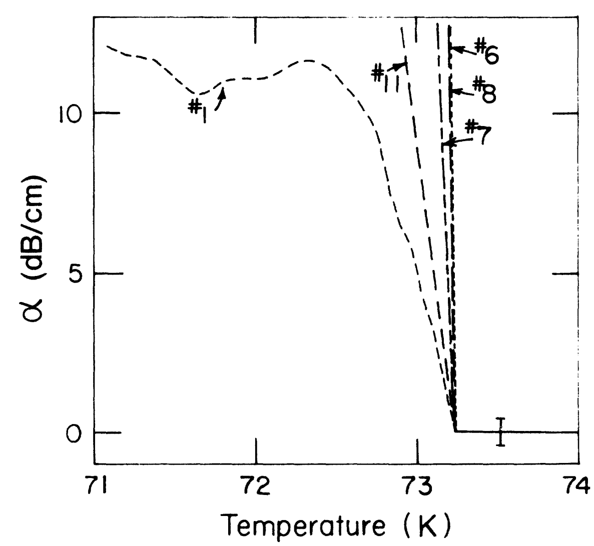

FIG. 11. Acoustic attenuation for several elastic modes below T_N. The mode numbers are given in Table I.

TABLE III. Comparison of the experimental and theoretical elastic stiffness moduli of NiF_2. Moduli are in units of 10^{11} dyn/cm^2.

Modulus	C_{11}	C_{33}	C_{44}	C_{66}	C_{12}	C_{13}
Experiment	14.50	22.08	4.65	9.94	11.0	9.09
Theory [a]	15.75	22.08	6.63	9.13	9.13	6.63
% diff.	+9%	0	+43%	−8%	−17%	−27%
Theory [b]	12.12	15.65	4.45	8.53	8.83	6.21
% diff.	−16%	−29%	−4%	−14%	−20%	−32%

[a] Predicted by using Pandey's method (see text).
[b] Predicted by Striefler and Barsch (Ref. 22).

models without considering the internal strains.

From the ir and the Raman frequencies, Striefler and Barsch[22] have determined the moduli of NiF_2. Their results are listed in Table III (b) for comparison. As can be seen, their values are all too small, especially for C_{33} and C_{13}. It has been pointed out by Traylor *et al.*[5] in connection with neutron dispersion experiments on rutile, that a shell model can predict dispersion curves in rutile better than rigid ion models. Neutron experiments and more theoretical work on NiF_2 are needed to explain the present observations.

B. Temperature dependence ($T > T_N$)

The temperature dependence of the elastic stiffness moduli for $T > T_N$ are presented in Figs. 2–5 and 10. Although $\Theta_D > 300$ K at room temperature, it is evident that each of the elastic moduli, except C_S, decreases as the temperature is increased at 300 K as is expected for $T \gtrsim \Theta_D$ from anharmonic lattice theories.[23]

The softening (decreasing) in C_S amounts to 5.5% from 300 K down to T_N. A few tens of degrees above T_N, there is a weak precursor which arrests its softening and, at and below T_N with a magnetic field present, there is tendency that the softening in the intrinsic C_S becomes totally arrested (see Fig. 8). If C_S is linearly extrapolated from between 300 and 90 K to $T = 0$ K, the extrapolated value at 0 K would be smaller than the value near T_N. This is unusual behavior. However, this would not happen if there is a concave downward curvature at some $T > 300$ K. Judging from the observed C_S softening behavior in rutile,[24] which has a Θ_D of 780 K and thermal expansion anomaly near 100 K and in MnF_2,[20] for which $\Theta_D = 370$ K and which has a magnetic phase transition at 66.5 K, we suggest that the C_S softening behavior in NiF_2 is the result of both the lattice instability (Born's criterion[16]) and the magnetic and/or structural phase transition at T_N. Furthermore, since there is evidence that the diamagnetic ZnF_2, which has no known phase transition below 300 K and an estimated Θ_D near 380 K, exhibits a softening in C_S with pressure at room temperature[25] similar to that observed in NiF_2,[13] we suggest that the softening of C_S in NiF_2 is mainly related to the lattice instability. Since the C_S mode induces e_{xx} and e_{yy} strains, any phase transition induced by this C_S softening may lower the crystal to a possible orthorhombic structure.

From Pandey's method to calculate C_S, it is found that C_S is determined by the force constant k'' which in term is determined by the Raman B_{1g} frequency. This prediction was verified in MnF_2. The measured B_{1g} frequency in MnF_2 decreases with temperature,[26] which implies that the force constant, and thus C_S, should decrease with temperature. This is exactly what has been observed.[20] Similarly, our observation of a decreasing C_S in NiF_2 predicts a decrease of the B_{1g} frequency by about 2.2% as T is lowered from 300 K to T_N. Unfortunately, Hutchings *et al.*[21] do not report the temperature dependence of the B_{1g} frequency in details.

C. Critical region

As shown in Figs. 6–10, C_{33}, C_{QL}, and C_{QS} (in the case of C_{QS}, a suitable magnetic field is required to locate the minimum) show typical inverted λ-type dips at 73.22 ± 0.05 K. In C_{44}, however, no local minimum at T_N was observed. The C_{44} curve goes smoothly through T_N with a rather broad maximum above T_N. One common feature of the above modes is the existence of long precursors of at least 100 deg above the phase transition (in the case of C_{44}, the precursor may also be related to the lattice instability). The strength of these dips is also large. For instance, the dip in C_{33} from its normal behavior assuming no phase transition is at least 2%. It was also observed that the attenuation maxima in mode C_{33}, C_{QL}, and C_{QS} are located at T_N. For C_{33} mode, the anomalous attenuation peak around T_N is about 1 dB/cm.

In contrast, C_{11}, C_{66}, and C_L show no precursor and no λ-type minimum near T_N.

It is clear that C_{33} is the only pure elastic mode which exhibits critical behavior near T_N. From current theories developed for critical phenomena, the acoustic velocity change Δv due to the coupling between the spin fluctuations and the acoustic wave in the critical region of ferromagnets or antiferromagnets has the form[27]

$$\Delta v \propto \epsilon^{-\zeta},$$

where $\epsilon = |T - T_N|/T_N$ is the reduced temperature parameter, ζ is the critical exponent. Although no such theory exists for weak ferromagnetic substances, an attempt was made to use the same formula to find the exponent for the velocity change in v_3. Using as background a simple linear extrapolation of the velocity from high temperature, the anomalous part of the velocity Δv_3 can be extracted. We found that ζ_+ above T_N is 0.068 ± 0.002 for $2.3\times10^{-4} < \epsilon < 1.8\times10^{-2}$ and ζ_- below T_N is 0.034 ± 0.003 for $2.4\times10^{-3} < \epsilon < 2.2\times10^{-2}$. A similar situation was also observed in antiferromagnetic MnF_2 or FeF_2,[3,28] in that ζ_+ is greater than ζ_- and both are smaller than the theoretical value.[3] However, when a magnetic field is turned on along the a direction, the dip becomes rounded and smeared (see Fig. 6), in which case, critical exponents cannot be found with certainty.

Since all the other pure shear modes such as C_{44}, C_{66}, and C_S do not show any λ-type singularity at T_N, we conclude that in the paramagnetic phase above T_N, the spin-phonon coupling mechanism is mainly volume magnetostrictive instead of linear magnetostrictive.[3] Furthermore, the volume magnetostrictive interaction in the paramagnetic phase is highly anisotropic because only the C_{33} mode exhibits a singularity but two other pure longitudinal modes, C_{11} and C_L, do not. From this behavior and using the formula derived by Kawasaki and Ikushima,[29] it is easy to conclude that $|\partial J_2/\partial a| > |\partial J_2/\partial c|$ in NiF_2 above T_N, where J_2 is the nearest-neighbor exchange interaction and a and c are the lattice constants.

D. Elastic behavior below T_N

C_{11}, C_{66}, C_L, and C_S exhibit drastic cutoff anomaly in zero magnetic field below T_N. As shown in Figs. 6–8, the anomalies in C_{11}, C_{22}, and C_S can be eliminated in a magnetic field of 4 kOe applied along the a direction, or in C_{66} and C_L along the [110] direction. Their behaviors in a magnetic field rotating in the a-b plane are shown qualitatively in Fig. 12 (b). All these behaviors can be explained by the magnetoelastic coupling effects.

By constructing a thermodynamic free energy containing magnetic, magnetoelastic, and elastic energy terms (neglecting the domain wall energies)

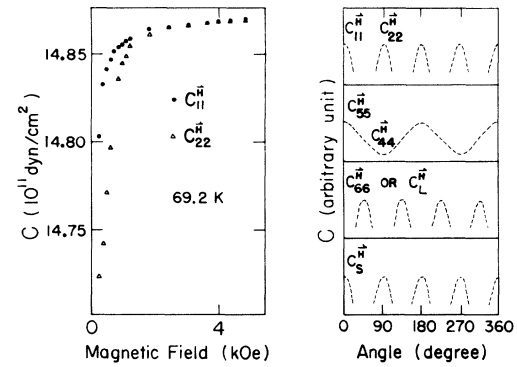

FIG. 12. (a) Behavior of C_{11} and C_{22} in magnetic fields applied along the a direction. (b) Schematic behaviors of several elastic modes in a magnetic field rotating in the a-b plane. Each in fixed temperature below T_N.

of the form

$$F = \vec{M}\cdot\vec{H}^* + \sum K_{ij}\alpha_i^2\alpha_j^2 + \sum B_{ij}\alpha_i\alpha_j e_{ij} + \frac{1}{2}\sum C_{ijkl}e_{kl}^2, \tag{1}$$

where $\vec{M}$ is the weak moment, $\vec{H}^*$ the effective magnetic field, α_i the direction cosine for the crystal i axis, K_{ij} the anisotropic energy, B_{ij} the magnetoelastic coupling constant, and e_{ij} the strain, it can be shown that the drop in the modulus C_{11} and C_S follow essentially a $\cos^2 2\theta/F(\theta)$ dependence, in C_{66} and C_L essentially a $\sin^2 2\theta/F(\theta)$ dependence, and in C_{55} (or C_{44}) essentially a $\cos^2\theta/F(\theta)$ dependence, where $F(\theta) = 2K_{11}\cos 4\theta + \vec{M}\cdot\vec{H}^*$, in agreement with our experimental observations qualitatively.

Below T_N in zero magnetic field, C_{12} also exhibits an anomaly. In fact, the C_{12} obtained from C_S increases and the C_{12} obtained from C_L decreases as the temperature is lowered below T_N. The plot in Fig. 10 shows only the average of these two values, which decreases. This interesting behavior is explained as follows: The change of C_{12} at constant $\vec{H}$ relative to its intrinsic value can be written[30]

$$\Delta C_{12} = \Delta[(S_{13}^2 - S_{12}S_{33})/\|S_{ij}\|],$$

where $i, j = 1, 2, 3$. By neglecting the small S_{13} and ΔS_{13} and using the compliances S_{ij}'s[31] calculated from the C_{ij}'s, we estimated that C_{12} increases if $|\Delta S_{12}/\Delta S_{11}| \geq 0.94$ or decreases if ≤ 0.94. This means that the stresses of the acoustic waves can develop some domain wall motions in the specimen such that the apparent compliances S_{11} and $-S_{12}$ become larger and more positive. But the magnitude of ΔS_{11} and ΔS_{12} may be different depending on the actual situation in the specimen. In the present observations, the condition ≥ 0.94 or ≤ 0.94 stated above may hold for C_S or C_L mode, respectively, at $\vec{H}=0$.

C_{13} is the average of the two C_{13}'s obtained from C_{QL} and C_{QS}. Its decreasing or increasing character below T_N is somewhat masked by the scattered data. Since C_{QL} and C_{QS} are quasimodes only, they can couple to other pure modes. The λ-type dips observed in these two modes are mainly the result of the coupling to the C_{33} mode, and the sharp cutoff anomaly observed at zero field in C_{QS} is mainly the result of the domain effect. This cutoff anomaly can be eliminated by applying a 4-kOe field along the *a* direction, as shown in Fig. 9. The domains in the crystal are randomly distributed in zero magnetic field. This can be seen from Fig. 7: When $\vec{H}=0$, the values C_{44} and C_{55} become equal and lie between those of C_{55} ($\hat{e} \parallel \vec{a}$) and C_{44} ($\hat{e} \parallel \vec{b}$).

From the above discussion, we suggest that the strong magnetoelastic coupling observed in C_{66} (C_{66} drops at least 7% in $\vec{H}=4$ kOe along the *a* direction) induces a possible shear instability in the crystal. The domains can be reorientated by a shear e_{xy} distortion and the twinlike domains are possible domain patterns in NiF_2. The boundary between twins can either be a Néel wall or a simple twin boundary parallel to the *c* axis. From symmetry consideration, the wall may preferably be parallel to the (110) plane. Of course, the domain patterns proposed by Moriya[7] in which domains are in forms of thin plates with the Bloch walls perpendicular to the *c* axis should not totally be excluded. The actual situation in NiF_2 may be a mixture of both possibilities which need further investigation.[32]

In principle, all the magnetoelastic coupling constants can be obtained by measuring the elastic moduli and the magnetostriction constants. The only measured magnetostriction constant is λ_{100} reported by Haefner *et al.*[9] By neglecting the magnetostriction along the *c* axis, it can be shown from Eq. (1) that λ_{100} and one of the magnetoelastic coupling constant B_{11} are related as

$$\lambda_{100} \approx \tfrac{1}{2} B_{11}/(C_{11}-C_{12}).$$

Since it is expected that the intrinsic $C_S = \frac{1}{2}(C_{11} - C_{12})$ does not change much below 65 K, using its value at 65 K and the reported λ_{100} value, we estimated $B_{11} \approx 8.5\times 10^7$ erg/cm^3 at 20.4 K.

ACKNOWLEDGMENTS

The author wishes to thank Professor J. C. Jamieson and Professor H. Fritzsche for their constant guidance, encouragement, and support during this research. Thanks are also due to Professor J. W. Stout, Professor O. J. Kleppa, and Professor J. R. Goldsmith for the use of their facilities; to Dr. J. Ito, T. N. Solberg, and M. C. Bachelder for specimen analysis; to S. A. Reed, D. Dennison, and J. Erwood for technical assistance.

---

†Research supported by the National Science Foundation Grant Nos. GA 16875, GA 147448, DES 73-00636 A02, and by the Air Force Office of Scientific Research under contract No. F44620-71-C-0025. We have also benefited from support of the Materials Research Laboratory by the NSF. Submitted in partial fulfillment of the requirements for the Ph.D. degree at The University of Chicago.

*Present address: Division of Chemistry, National Research Council of Canada, Ottawa K1A 0R9, Canada.

[1]H. J. McSkimin, J. Acoust. Soc. Am. 22, 413 (1950).

[2]H. J. McSkimin, J. Acoust. Soc. Am. 33, 12 (1961).

[3]B. Lüthi, T. J. Moran, and R. J. Pollina, J. Phys. Chem. Solids 31, 1741 (1970).

[4]C. W. Garland, in *Physical Acoustics*, edited by W. P. Mason and R. N. Thurston (Academic, New York, 1970), Vol. VII.

[5]J. G. Traylor, H. G. Smith, R. M. Nicklow, and M. K. Wilkinson, Phys. Rev. B 3, 3457 (1971).

[6]I. E. Kzialoshinskii, Zh. Eksp. Teor. Fiz. 33, 1454 (1957) [Sov. Phys.-JETP 6, 1120 (1958)].

[7]T. Moriya, Phys. Rev. 117, 635 (1960).

[8]See, for example, K. P. Belov and A. M. Kadomtseva, Usp. Fiz. Nauk 103, 577 (1971) [Sov. Phys.-Usp. 14, 154 (1971)].

[9]K. Haefner, J. W. Stout, and C. S. Barrett, J. Appl. Phys. 37, 449 (1966).

[10]W. H. Baur, Acta Crystallogr. 11, 488 (1958).

[11]S. J. Joshua and A. P. Cracknell, J. Phys. C 2, 24 (1969).

[12]A. Y. Wu (unpublished).

[13]A. Y. Wu (unpublished).

[14]We used the sine burst generator manufactured by the PM Custom Electronics.

[15]W. P. Mason, *Physical Acoustics and the Properties of Solids* (Van Nostrand, New York, 1958), p. 369.

[16]M. Born and K. Huang, *Dynamical Theory of Crystal Lattices* (Oxford University, London, 1968), Chap. III.

[17]D. D. Betts, A. B. Bhatia, and G. K. Horton, Phys. Rev. 104, 43 (1956).

[18]F. Matossi, J. Chem. Phys. 19, 1543 (1951).

[19]H. N. Pandey, Phys. Status Solidi 11, 743 (1965).

[20]R. L. Melcher, Phys. Rev. B 2, 733 (1970).

[21]M. T. Hutchings, M. F. Thorpe, R. J. Birgeneau, P. A. Fleury, and H. J. Guggenheim, Phys. Rev. B 2, 1362 (1970). Although their reported Raman frequencies are actually at 80 K, we adopted them to calculated the elastic moduli at room temperature. This should be a good approximation for our present purpose.

[22]M. E. Striefler and G. R. Barsch, Phys. Status Solidi B 59, 205 (1973).

[23]G. Leibfried and W. Ludwig, in *Solid State Physics*,

edited by F. Seitz and D. Turnbull (Academic, New York, 1961), Vol. 12.

[24]M. H. Manghnani, E. S. Fisher, and W. S. Brower, Jr., J. Phys. Chem. Solids 33, 2149 (1972).

[25]M. E. Striefler and G. R. Barsch, Phys. Status Solidi B 64, 613 (1974).

[26]S. P. S. Porto, P. A. Fleury, and T. C. Damen, Phys. Rev. 154, 522 (1967).

[27]H. S. Bennett, Phys. Rev. 185, 801 (1969).

[28]A. Ikushima, J. Phys. Chem. Solids 31, 283 (1970); 32, 417 (1971).

[29]K. Kawasaki and A. Ikushima, Phys. Rev. B 1, 3143 (1970).

[30]Similar arguments have been made by C. Kittel [Comments Solid State Phys. 2, 47 (1972)] in studying domain effects in ferroelectric $SrTiO_3$.

[31]Determined from C_{ij}'s, the elastic compliance moduli in NiF_2 at 74 K are, in units of 10^{-12} cm^2/dyn, $S_{11}=1.81$, $S_{12}=-1.27$, $S_{13}=-0.23$, $S_{33}=0.66$, $S_{44}=2.14$, and $S_{66}=0.96$.

[32]A. Y. Wu (unpublished).